Inducing an optical Feshbach resonance via stimulated Raman coupling

Gregor Thalhammer,[1] Matthias Theis,[1] Klaus Winkler,[1] Rudolf Grimm,[1,2] and Johannes Hecker Denschlag[1]
[1]*Institut für Experimentalphysik, Universität Innsbruck, Technikerstraße 25, 6020 Innsbruck, Austria*
[2]*Institut für Quantenoptik und Quanteninformation, Österreichische Akademie der Wissenschaften, 6020 Innsbruck, Austria*
(Received 23 September 2004; published 8 March 2005; publisher error corrected 11 March 2005)

We demonstrate a method of inducing an optical Feshbach resonance based on a coherent free-bound stimulated Raman transition. In our experiment atoms in a ^{87}Rb Bose-Einstein condensate are exposed to two phase-locked Raman laser beams which couple pairs of colliding atoms to a molecular ground state. By controlling the power and relative detuning of the two laser beams, we can change the atomic scattering length considerably. The dependence of scattering length on these parameters is studied experimentally and modeled theoretically.

DOI: 10.1103/PhysRevA.71.033403 PACS number(s): 34.50.Rk, 32.80.Pj, 03.75.Nt, 34.20.Cf

I. INTRODUCTION

Feshbach resonances have become a central tool in the physics of ultracold quantum gases during the last years because they allow for a tuning of the interactions between atoms. Controlling interparticle interactions is a central key in many fields of modern physics and is especially relevant for future applications in quantum computation and exploring novel many-particle quantum effects. Beautiful experiments using magnetically tunable Feshbach resonances [1,2] have been performed, ranging from ultrahigh-resolution molecular spectroscopy [3] to the coherent coupling of atomic and molecular states [4] as well as the creation of bright matter wave solitons [5]. It also led to the production of new atomic [6] and molecular [7] Bose-Einstein condensates (BEC's) and allowed control of pairing in ultracold fermionic gases [8].

Recently we demonstrated how atom-atom interactions in a ^{87}Rb BEC can also be tuned with an optically induced Feshbach resonance [9] (see also [10]), a scheme which was originally proposed by Fedichev *et al.* [11,12]. Optically induced Feshbach resonances offer advantages over magnetically tuned Feshbach resonances since the intensity and detuning of optical fields can be rapidly changed. Furthermore, complex spatial intensity distributions can be easily produced and optical transitions are always available even when no magnetic Feshbach resonances exist. A disadvantage of optically induced Feshbach resonance is the inherent loss of atoms due to excitation and spontaneous decay of the molecular state [9]. Typical lifetimes for excited molecular states are on the order of 10 ns which corresponds to a linewidth of $2\pi\times 16\,\mathrm{MHz}$. Evidently, coupling to molecular states with longer lifetime should improve the situation. Ground-state molecules are stable against radiative decay, and narrow transition linewidths on the order of kHz have been observed in two-photon Raman photoassociation [13,14]. This raises the question whether it is possible to create optical Feshbach resonances using stimulated Raman transitions and whether this scheme might be advantageous compared to the one-photon optical Feshbach resonance.

In this paper we indeed demonstrate that optical Feshbach resonances can be induced using a coherent two-color Raman transition to a highly vibrationally excited molecular ground state in a ^{87}Rb BEC. In the experiment we show how the scattering length and loss rates can be tuned as a function of the intensity of the lasers and their detuning from molecular lines. We use Bragg spectroscopy [15] as a fast method to measure the scattering length in our sample [9]. To fit and analyze our data we use a model by Bohn and Julienne [16]. We find that using the Raman scheme for optically induced Feshbach resonances leads to similar results in tuning of the scattering length as for the single-photon Feshbach scheme. The Raman scheme does not lead to an improvement compared to the one-photon scheme because its atomic loss rate is not lower for a given change in scattering length. However, using a stimulated Raman transition does offer experimental advantages. To tune over the Feshbach resonance, the relative frequency of the two laser beams only has to be changed typically by several MHz which can be conveniently done using an acousto-optic modulator. This allows for very fast and precise control of the scattering length. On the other hand, working with a one-photon optical Feshbach resonance in the low-loss regime typically requires large detunings and scan ranges on the order of GHz. The Raman scheme relaxes the necessity for absolute frequency control of the lasers which can be tedious to maintain far away from atomic lines. Since off-resonant light fields in general lead to dipole forces acting on the atoms, a variation of the scattering length via optical tuning leads to a variation of the dipole forces on the atomic sample. This unwanted effect can be made negligible for the Raman scheme which tunes over resonance within a small frequency range.

The paper is organized as follows: We start in Sec. II by discussing the Raman scheme with a simple theoretical model. In Sec. III we describe in detail our experimental setup and the measurement method. In Sec. IV we discuss the experimental results which are compared with a theoretical model. The Appendix gives details of the model that is used to describe the data.

II. RAMAN SCHEME FOR OPTICAL FESHBACH TUNING

Before discussing optical Feshbach tuning based on a two-photon Raman transition, it is instructive to briefly recall

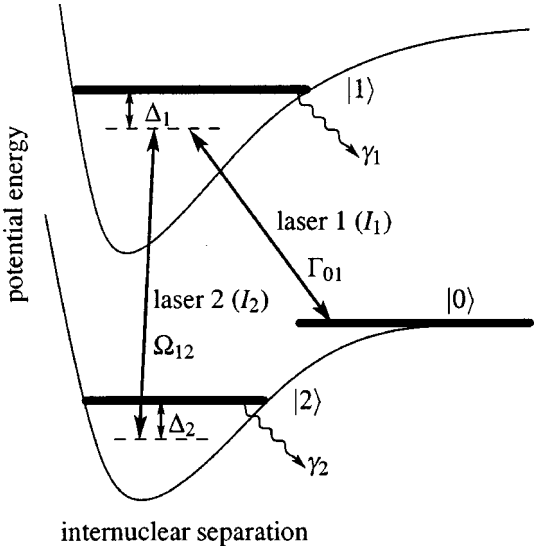

FIG. 1. Schematic diagram of the transitions used for optically coupling the collisional state $|0\rangle$ to molecular states $|1\rangle$ and $|2\rangle$. $|1\rangle$ is electronically excited whereas $|2\rangle$ is in the electronic ground state. Δ_1 and Δ_2 are defined to be positive for the shown configuration.

the one-photon scheme first [9,11,12]. This configuration uses a single laser beam tuned close to a transition from the scattering state of colliding atoms to a bound level in an excited molecular potential (states $|0\rangle$ and $|1\rangle$ in Fig. 1). Varying the detuning Δ_1 or the intensity I_1 modifies the coupling and hence the scattering length. Atomic loss can occur through population of the electronically excited molecular state which has a decay width of γ_1.

Introducing a second laser as shown in Fig. 1 will now couple the collisional state $|0\rangle$ to a bound level $|2\rangle$ in the ground-state potential. As we will show, this allows for a tuning of the scattering length similar to the one-photon scheme. We now have, however, four parameters which can be used to influence the scattering length: the intensities I_1 and I_2 of lasers 1 and 2 and the detunings Δ_1 and Δ_2 as shown in Fig. 1.[1]

From [16] [Eqs. (4.8)–(4.11)] one can extract approximate expressions for the inelastic collision rate coefficient K_{inel} and the scattering length a in a Bose-Einstein condensate:[2]

$$K_{\text{inel}} = \frac{2\pi\hbar}{m}\frac{1}{k_{\text{i}}}\frac{\Gamma_{01}\gamma_1}{(\Delta_1 - \Omega_{12}^2/\Delta_2)^2 + (\gamma_1/2)^2}, \tag{1}$$

[1]As we observe a significant light shift of level $|1\rangle$, depending on the intensity I_1 of laser 1 [9], we measure the detuning Δ_1 from the observed position of the one-photon line at a given intensity of laser 1. Note that Δ_1 is a one-photon detuning whereas Δ_2 is a two-photon detuning.

[2]K_{inel} is reduced by a factor of 2 as compared to the case of thermal atoms. This is because in a BEC all atoms share the same quantum state.

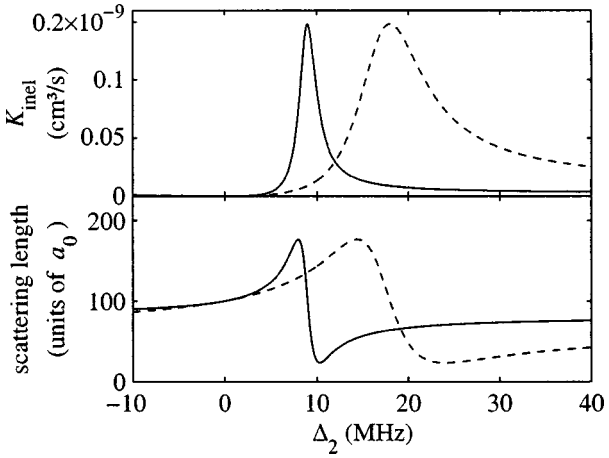

FIG. 2. K_{inel} and scattering length a according to Eqs. (1) and (2), plotted for two values of Δ_1. Solid line: $\Delta_1/2\pi = 100$ MHz. Dashed line: $\Delta_1/2\pi = 50$ MHz. The other parameters are $\Gamma_{01}/2\pi = 50$ kHz, $\Omega_{12}/2\pi = 30$ MHz, and $\gamma_1/2\pi = 25$ MHz. The wave number $k_{\text{i}} = 2.5\times10^5$ m^{-1} corresponds to the finite size of the condensate wave function. a_0 is the Bohr radius.

$$a = a_{\text{bg}} - \frac{1}{2k_{\text{i}}}\frac{\Gamma_{01}(\Delta_1 - \Omega_{12}^2/\Delta_2)}{(\Delta_1 - \Omega_{12}^2/\Delta_2)^2 + (\gamma_1/2)^2}. \tag{2}$$

Here Γ_{01} denotes the on-resonance stimulated transition rate from $|0\rangle$ to $|1\rangle$ which is proportional to I_1. Ω_{12} is the Rabi frequency for the coupling of the states $|1\rangle$ and $|2\rangle$ and is proportional to $\sqrt{I_2}$. $\hbar k_{\text{i}}$ is the relative momentum of the collision, where $\hbar$ is Planck's constant divided by 2π. a_{bg} is the background scattering length and m is the atomic mass.

Equations (1) and (2) neglect spontaneous decay from state $|2\rangle$ ($\gamma_2 = 0$) and assume $\Gamma_{01} \ll \gamma_1$. Setting $\Omega_{12} = 0$ yields the expressions for the one-photon Feshbach resonance as given in [9]. Equations (1) and (2) yield a Lorentzian and a corresponding dispersive line shape as a function of Δ_1. In our experiments, however, we hold Δ_1 constant and scan Δ_2. Figure 2 shows typical curves for K_{inel} and a for two detunings Δ_1. The curves for K_{inel} are slightly asymmetric, but for $\Delta_1 \gg \Omega_{12}$ they can be well approximated by Lorentzians. This can be seen by expanding the denominator of Eq. (1) in terms of Δ_2 at the resonance position. A light shift displaces the position of the resonance to ${\Omega_{12}}^2/\Delta_1$. It is also interesting to note that the resonance width decreases with increasing detuning Δ_1 as $\gamma_1(\Omega_{12}/\Delta_1)^2$.

In a sense the two-photon Raman-Feshbach resonance can be coined in terms of a one-photon Feshbach scheme. The detuning Δ_2 effectively replaces the detuning Δ_1 of the one-photon Feshbach scheme.[3]

Since Eqs. (1) and (2) have exactly the same form as for the one-photon Feshbach resonance, it follows that, given a

[3]There is even a more direct way to understand the two-photon Feshbach resonance in terms of a one-photon Feshbach resonance. Laser 1 couples the collision state $|0\rangle$ to a virtual level $|2'\rangle$, which is generated by laser 2 acting on level $|2\rangle$. The splitting between $|2'\rangle$ and $|1\rangle$ is given by $\Delta_{2'} = \Delta_1 - \Delta_2$. Its linewidth is $\gamma_1(\Omega_{12}/\Delta_{2'})^2$ and the transition rate $\Gamma_{02'} = \Gamma_{01}(\Omega_{12}/\Delta_{2'})^2$.

fixed free-bound transition rate Γ_{01}, the maximum tuning range of the scattering length for the two-photon case cannot be larger than in a one-photon scheme. Furthermore, given a fixed change in scattering length, the loss rate as determined by K_{inel} is not lower for the Raman scheme than for the one-photon scheme.

III. EXPERIMENTAL SETUP AND METHODS

A. Production of BEC's

For the experiments we produce ^{87}Rb BEC's of typically 1.2×10^6 atoms in the spin state $|F=1,m_F=-1\rangle$. Our setup comprises a magnetic transfer line [17] to transport atoms from a magneto-optic trap (MOT) chamber to a glass cell where the BEC is produced and all experiments are carried out. In a first step about 3×10^9 atoms are loaded within 4 s into a MOT directly from the background gas and are then cooled further to about 50 μK in a molasses cooling phase. After optically pumping into the $|F=1,m_F=-1\rangle$ state we load the atom cloud into a magnetic quadrupole trap with a gradient of 130 G/cm in the (strong) vertical direction. Within 1.4 s the atoms are then moved via a magnetic transfer line[4] over a distance of 48 cm including a 120° corner into a glass cell which is at a pressure below 10^{-11} mbar. In this cell we finally load the cloud into a QUIC trap (a type of magnetic trap that incorporates the quadrupole and Ioffe configuration) [18], ending up with typically 4×10^8 atoms at a temperature of about 250 μK. All three coils of the QUIC trap are operated at a current of 40 A, dissipating 350 W. This results in trap frequencies of $\omega_{\mathrm{radial}}/2\pi=150$ Hz and $\omega_{\mathrm{axial}}/2\pi=15$ Hz at a magnetic bias field of 2 G. To achieve Bose-Einstein condensation we use forced radio-frequency evaporation for a period of 20 s. The stop frequency is chosen so that we end up with condensates with a thermal background of about 25% of noncondensed atoms. At this value we concurrently get the highest number of atoms in the condensate and good reproducibility. For our measurements we consider only the condensed atoms.

B. Raman lasers

To realize the Raman scheme shown in Fig. 1 we use the electronically excited molecular state $|1\rangle=|0_g^-,\ \nu=1,\ J=2\rangle$ located 26.8 cm^{-1} below the $(S_{1/2}+P_{3/2})$ dissociation asymptote [9,19]. About 290 MHz below the $J=2$ line, there is another rotational level with $J=0$.[5] Although about 5 times weaker than the $J=2$ line, its effect cannot be totally neglected in our experiment. We choose level $|2\rangle$ to be the second to last bound state in the ground-state potential. It has a binding energy of 636 MHz$\times h$ [13] where h is Planck's constant.

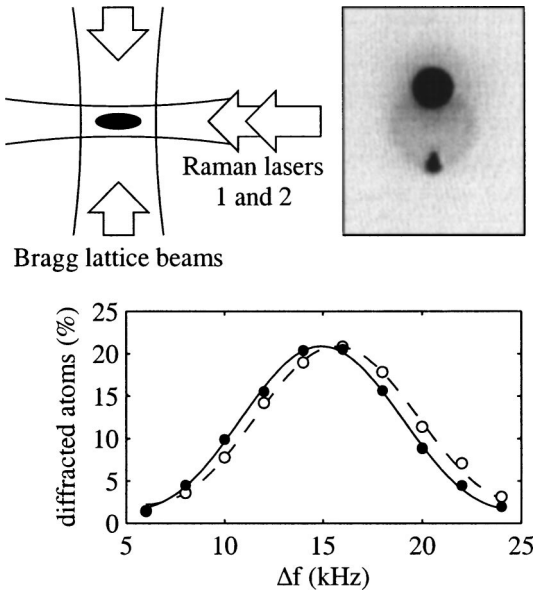

FIG. 3. Top left: experimental arrangement of the laser beams (top view). Top right: absorption image obtained after Bragg-diffracting a portion of the atoms to a state with a momentum of two photon recoils (lower atom cloud) and subsequent time of flight expansion. Bottom: Bragg resonance curves for two different relative detunings of the Raman lasers. The relative shift of 700 Hz is due to two different scattering lengths which are optically induced in the condensates. The atom numbers are the same for both curves. Shown is the percentage of diffracted atoms versus the frequency difference of the Bragg lattice beams. For better comparison we have scaled up the right curve by 10%.

The Raman laser beams are derived from a Ti:sapphire laser using an acousto-optical modulator at a center frequency of about 318 MHz in a double-pass configuration. This allows precise control of their relative frequency difference over several tens of MHz. Both Raman lasers propagate collinearly and are aligned along the weak axis of the magnetic trap (see Fig. 3). They have a $1/e^2$ waist of 76 μm, and their linear polarization is perpendicular to the magnetic bias field of the trap.

The Ti:sapphire laser is intensity stabilized and its frequency has a linewidth of about 3 MHz. In order to stabilize its frequency relative to the photoassociation lines, the laser is offset locked relative to the D_2 line of atomic rubidium with the help of a scanning optical cavity. This yields an absolute frequency accuracy of better than 10 MHz. In all our experiments the Raman laser intensities were set to $I_1=300$ W/cm^2 and $I_2=60$ W/cm^2 at the location of the condensate, if not stated otherwise.

C. Bragg spectroscopy

To measure optically induced changes in the scattering length a, we use Bragg spectroscopy [9,15]. This method allows for a fast measurement on time scales below 100 μs which is vital because of the rapid photoassociation losses

[4]For our magnetic transport (similar to that described in [17]) 13 pairs of quadrupole coils are used. These transfer coils each have an inner diameter of 23.6 mm, an outer diameter of 65 mm, and a height of 5.7 mm and consist of 34 windings. They are arranged in two layers above and below the vacuum chamber with a separation of 50 mm. Peak currents of 75 A are necessary to maintain a vertical gradient of 130 G/cm during transfer.

[5]Due to different light shifts [9] for the $J=0$ and $J=2$ lines, their splitting is intensity dependent. The value of 290 MHz is valid for an intensity of 300 W/cm^2.

we experience in our experiments. A moving lattice composed of two counter propagating beams with wave number k and a frequency difference Δf is used to diffract some of the condensate atoms to a state with nonzero momentum. When energy and momentum conservation are fulfilled, the Bragg lattice resonantly transfers a momentum of two photon recoils $2\hbar k$ in a first-order diffraction process. For the case of a homogeneous condensate of density n, the resonance energy for Bragg diffraction is given by the sum of transferred kinetic energy $h\Delta f_0=(2\hbar k)^2/2m$ and the change in mean-field energy $4\pi\hbar^2 na/m$.[6] This corresponds to a frequency difference of the Bragg lasers of

$$\Delta f_r = \Delta f_0 + \frac{2\hbar}{m} na. \tag{3}$$

If the condensate is initially not at rest, the kinetic energy contribution Δf_0 to the Bragg resonance frequency [Eq. (3)] contains an additional term $2\hbar kp/m$, where p is the initial atom momentum in the direction of the Bragg lattice. In our experiments we observe such a motional shift corresponding to condensate momentum of up to $p=0.1\ \hbar k$. This momentum can partly be attributed to optical dipole forces of Raman beams which are slightly noncentered on the condensate. Partly it can be attributed to a forced oscillation of the condensate in the magnetic trap at 150 Hz which coincides with the trapping frequency. Since this oscillation is driven by a higher harmonic of the line frequency (50 Hz), it is in phase with the line frequency and we are able to stabilize the initial condensate momentum by synchronizing the experiment to the line. A stable initial condensate momentum can then be determined and canceled out by measuring Δf_r alternately for Bragg diffraction to the $+2\hbar k$ and $-2\hbar k$ momentum components. After these measures we were left with a residual momentum noise level of up to $p=0.01\ \hbar k$.

In our setup the Bragg lattice beams are oriented along the horizontal direction perpendicular to the Raman laser beams (see Fig. 3) and have a width of ≈ 0.9 mm. We extract both beams from a single grating-stabilized diode laser and use two acousto-optical modulators to control the frequency difference. The laser is tuned 1.4 nm below the ^{87}Rb D_2 line which defines Δf_0 in Eq. (3) to be 15.14 kHz. This frequency is much larger than the typical mean-field contribution, $2\hbar na/m$, which in our experiments was below 3 kHz.

We illuminate the trapped condensate for 100 μs with the Bragg lattice light. After 12 ms of free expansion the diffracted atoms are spatially separated from the remaining atoms. Absorption imaging allows us to determine the diffraction efficiency. By adjusting the Bragg laser intensity (typically 1 mW) we keep the maximum diffraction efficiency between 15% and 20%. When we scan the frequency difference Δf and measure the fraction of Bragg-diffracted atoms we obtain curves as shown in Fig. 3 (bottom). These curves have a width of approximately 9 kHz as determined by the 100 μs length of our Bragg pulses. The shape of the curves is given by the Fourier transform of our square light pulses which we use to fit the data to obtain the resonance position Δf_r [9]. The shift between the two Bragg spectroscopy curves in Fig. 3 (bottom) is optically induced by shining in the Raman lasers at the same time as the Bragg lattice. For both curves the atom numbers are the same and $\Delta_1 = 60$ MHz. Only the Raman detuning Δ_2 differs by 26 MHz. According to Eq. (3) this observed shift in Bragg resonance frequency is then due to a change in scattering length, induced by tuning Δ_2. This demonstrates that we can tune the scattering length a with a Raman Feshbach resonance.

D. Determination of scattering length

We use Eq. (3) to determine the scattering length a from the measurements of the Bragg resonance frequency Δf_r. Equation (3), however, is derived for the case of a homogeneous condensate. Our trapped condensate, in contrast, which is subject to photoassociation losses, exhibits a time- and position-dependent density n. This can be taken into account by replacing the density n in Eq. (3) by an appropriate effective value $\bar{n}$.

A simple approach to estimate $\bar{n}$ is to calculate the spatial and time average of the condensate density n over the duration of the Raman pulse length T. For this we use the rate equation for the local density $\dot{n}=-2K_{\mathrm{inel}}n^2$ for two-atom losses. The inelastic collision rate coefficient K_{inel} governing this process is obtained from measuring the atom number at the beginning and end of the light pulse. This procedure already yields good results which differ less than 10% from an improved approach which we use for our data analysis and which is explained in the following.

The improved approach consists of a full numerical simulation which describes Bragg diffraction in a dynamically and spatially resolved way. We divide the condensate into density classes and treat their time dependence individually. The Bragg diffraction process is identified as a Rabi oscillation between a coherent two level system—i.e., the BEC component at rest and the Bragg-diffracted component. The changing density of the condensate due to loss is reflected in a time-dependent resonance frequency [see Eq. (3)]. As a result of these calculations we obtain for each density class a Bragg resonance curve similar to the experimental ones shown in Fig. 3. Averaging over these resonance curves and determining the center position yields the simulated value for the Bragg resonance Δf_r. Using $\Delta f_r=\Delta f_0+2\hbar\bar{n}a/m$ we can then determine the effective density $\bar{n}$.

IV. RESULTS

A. Raman scans

Figure 4 presents measurements where the detuning Δ_1 of laser 1 from the excited molecular state is set to $\Delta_1/2\pi = 60$ MHz. The intensities of the Raman lasers 1 and 2 are 300 W/cm^2 and 60 W/cm^2, respectively. Figure 4(a) shows the atom number after illuminating a condensate of initially 1.4×10^6 atoms for 100 μs with the Raman lasers. Scanning the Raman detuning Δ_2 we find a strong loss of atoms on resonance. As already expected from Eq. (1) the line shape is slightly asymmetric. Figure 4(b) shows the resonance fre-

[6]This is valid in the limit that only a small fraction of the condensate is diffracted.

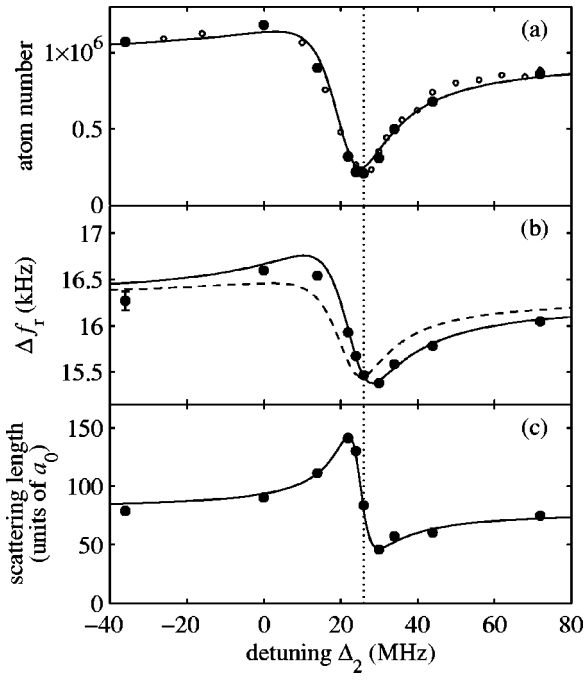

FIG. 4. Optical Feshbach resonance using a Raman scheme. (a) shows the measured atom number after the Raman pulse, (b) the measured Bragg resonance frequency, and (c) the scattering length, as determined from (a) and (b). In (a) the solid circles correspond to measurements where Bragg spectroscopy was used to determine the scattering length, while the small open circles stem from additional loss measurements without Bragg spectroscopy. From our measurements we estimate the uncertainty of the Bragg resonance frequency to be smaller then ±100 Hz, as indicated by the error bar in (b). The solid lines in (a), (b), and (c) are from a model calculation (see the Appendix and text). The dashed line in (b) shows the expected signal if there was only loss in atom number but no change in scattering length (see also discussion in text). The vertical line indicates the location of maximal loss in (a) and helps to compare the relative positions of the three curves.

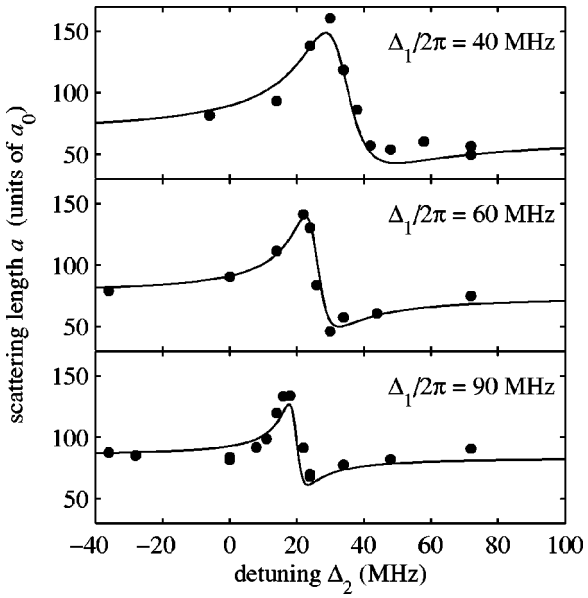

FIG. 5. Variation of the scattering length with Raman detuning for three various detunings Δ_1 from the excited molecular state. The solid line is a calculation (see the Appendix) which uses a single set of parameters for all curves.

quency Δf_r as measured by Bragg spectroscopy. When we analyze the data in Figs. 4(a) and 4(b) with the improved procedure described in Sec. III D we obtain values for the scattering length which are shown in Fig. 4(c). The scattering length a shows a dispersive variation between $50\,a_0$ and $140\,a_0$ as we scan over the resonance. The dispersive scattering length curve is offset by about $20\,a_0$ from the background scattering length $a_{bg}=100\,a_0$ for ^{87}Rb in the $|F=1, m_F=-1\rangle$ state [20–22]. This is due to the one-photon Feshbach tuning of laser 1, in agreement with our previous measurements [9].

We find that Eqs. (1) and (2) are not sufficient to describe these data properly, mainly because they neglect the decay rate γ_2. A more complete model (see the Appendix), also taking into account both the $J=0$ and $J=2$ rotational levels, was used for creating fit curves,[7] depicted as solid lines in Fig. 4. The fact that the data for atomic loss as well as for the scattering length a are both well described by the theoretical curves is an intrinsic consistency check for our model and our data analysis.

The shape of the signal Δf_r in Fig. 4(b) is a combination of the effects of the varying scattering length a and the varying atom number [see Eq. (3)]. This is illustrated by the dashed and continuous lines in Fig. 4(b): The dashed line shows the expected signal if only the variations in atom number would occur and the scattering length stayed constant.[8] The solid line takes the variations in both atom number and scattering length into account. The deviation of the measured data points from the dashed line is due to an optical induced change of the scattering length.

B. Dependence on detuning

We now investigate how detuning Δ_1 affects the scattering length a. Figure 5 shows a set of three curves showing the scattering length for detunings $\Delta_1/2\pi=40$, 60, and 90 MHz.

The measurements clearly show that the position and width of the resonances depend on Δ_1. The change in position can be mainly explained as light shifts of levels $|1\rangle$ and $|2\rangle$ due to laser 2. The decrease of the resonance width with increasing detuning Δ_1 follows directly our discussion in Sec. II. The solid lines are model calculations as described in detail in the Appendix. They are derived from a simultaneous fit to the data shown in Fig. 5 and a large number of atom loss measurements with different detunings (not shown). The set of fit parameters is listed in the Appendix. We also use this same set of parameters for the theoretical curves in Figs. 6 and 7.

[7]The resulting fit parameters are similar to those given in the Appendix.

[8]To account for the one-photon Feshbach tuning of laser 1, a value for the background scattering length $a_{bg}=80\,a_0$ was used for the calculation.

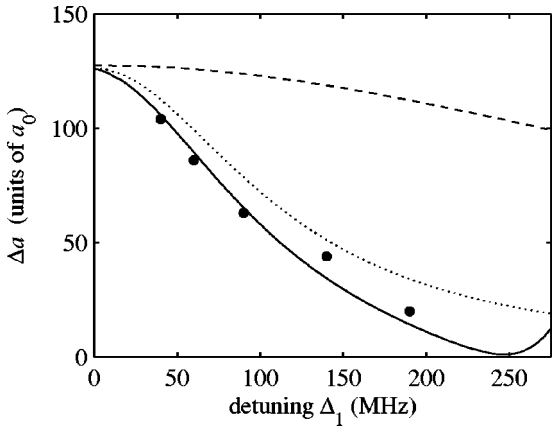

FIG. 6. Maximum variation in scattering length $\Delta a = a_{\max} - a_{\min}$ versus one-photon detuning Δ_1. Solid line: full model calculation (see the Appendix). Dotted line: three-level model (see Fig. 1), with $\gamma_2/2\pi = 2$ MHz. Dashed line: three-level model, with $\gamma_2/2\pi = 100$ kHz.

It is interesting to note from Fig. 5 that the amplitude of the dispersive scattering length signal decreases as Δ_1 becomes larger. This is not to be expected from the simple model Eqs. (1) and (2). To investigate this effect we have performed scans for atom loss and scattering length for several detunings Δ_1. Figure 6 shows the maximum variation in scattering length, $\Delta a = a_{\max} - a_{\min}$, obtained for detunings Δ_1 ranging from 40 MHz to 200 MHz. Here, $a_{\max}$ and $a_{\min}$ are the maximal and minimal scattering length values for corresponding scan curves. Typical scan curves are shown in Fig. 5. Each data point in Fig. 6 was derived from a complete scan and corresponds to one day of data collection.

An analysis of our data using our theoretical model indicates that the decrease of Δa as a function of Δ_1 is a consequence of two effects.

(i) To properly model these measurements we have to assign to the molecular state $|2\rangle$ in the ground-state potential a non-negligible decay width $\gamma_2/2\pi \approx 2$ MHz. For comparison, two calculations of a three-level model are plotted in Fig. 6. For small $\gamma_2/2\pi = 100$ kHz (dashed line) Δa decreases only weakly. For $\gamma_2/2\pi = 2$ MHz (dotted line) the theory fits the data much better. Such a large decay rate of a ground-state level is surprising. It seems too large to be explained purely by collisions. We find that the decay rate increases with the light intensity. At low light powers of a few W/cm^2 we have observed very narrow linewidths $\gamma_2/2\pi$ on the order of a few kHz, similar to the values reported by [13,14]. The broadening of the molecular ground level could be due to coupling to excited molecular levels. We can exclude, however, from our experimental data that these levels are located within our experimental scanning range between the states $|1\rangle$ and $|3\rangle$. This would lead to additional resonance features in the scattering length, absorption, and light shifts, which are inconsistent with our data. In contrast, our data indicate a relatively constant background loss rate of the ground level over the experimental scan range. This allows us to analyze the data successfully with our simple few-level model. Besides coupling to excited molecular states, we suspect that coupling to the *d*-wave shape resonance of the scattering channel also gives rise to a sizable contribution to the molecular decay rate. Because the *d*-wave shape resonance is located very close (a few MHz) to threshold, it is resonantly coupled to the molecular ground-state level via the Raman transition. To include the shape resonance is beyond the reach of our simple model and has to be investigated later.

(ii) The second reason for the decrease in Δa is a quantum interference effect involving both the $J=2$ and $J=0$ rotational levels as predicted by our model. At a detuning of $\Delta_1/2\pi \approx 250$ MHz the interference effect leads to a complete disappearance of the optical Feshbach resonance. We observe this in a corresponding disappearance of the atom loss feature in our measurements (not shown). The interference effect alone—i.e., without a 2 MHz linewidth—is not sufficient to explain the experimental data in Fig. 6.

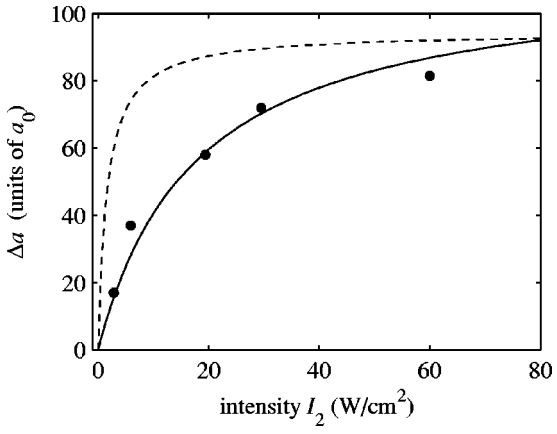

FIG. 7. Maximum variation in scattering length $\Delta a = a_{\max} - a_{\min}$ versus I_2. For this data set $I_1 = 300$ W/cm^2 and $\Delta_1 = 60$ MHz. The solid line is a full model calculation (see the Appendix). The dashed line stems from the same model, but with $\gamma_2/2\pi$ set to 100 kHz and is scaled by a factor of 0.84 for better comparison.

C. Dependence on intensity

From the simple model Eq. (2) it is clear that the maximum variation in scattering length Δa is proportional to Γ_{01} and consequently scales linearly with the intensity I_1 of laser 1. We have verified this dependence recently [9] for the case of a one-photon optical Feshbach resonance.

In contrast, the dependence of Δa on intensity I_2 of laser 2 is not so trivial. According to the simple model, Eqs. (1) and (2), which neglects the decay rate γ_2, the maximum change Δa is independent of I_2. It is also clear, that for $I_2 = 0$ we have $\Delta a = 0$ since there is no dependence of scattering length on Δ_2 at all. This unphysical discontinuous behavior can be resolved if we introduce a finite decay rate $\gamma_2 > 0$. We then find that for increasing intensity $I_2, \Delta a$ rises monotonously from zero to a value where it saturates. We observe this general behavior in our measurements presented in Fig. 7. Our full model, as described in the Appendix, describes the measured data well if we set the decay rate to $\gamma_2/2\pi = 2$ MHz (solid line). In contrast, the dashed line in Fig. 7 shows the calculation for the same model where γ_2 is set to

$\gamma_2/2\pi=100$ kHz. Saturation then occurs at a much lower intensity I_2 than for $\gamma_2/2\pi=2$ MHz.

V. CONCLUSION

Our experiments demonstrate the use of an optical Feshbach resonance for tuning of the scattering length via stimulated Raman coupling to a bound molecular state. Our results show that there is no advantage over a one-photon scheme when comparing tuning range and loss rate. However, for certain applications a Raman scheme is experimentally more favorable since it demands a lower tuning range of the lasers. Our presented theoretical model is in good agreement with our data and might be helpful when tailoring experimental parameters for a specific application. Furthermore, it gives insight into the process of creating stable ultracold molecules via two-photon photoassociation.

ACKNOWLEDGMENTS

We appreciate the help of George Ruff and Michael Hellwig at an early stage of the experiment. We thank Paul Julienne, Eite Tiesinga, John Bohn, Olivier Dulieu, Peter Fedichev, Andrea Micheli, and Helmut Ritsch for valuable discussions. This work was supported by the Austrian Science Fund (FWF) within SFB 15 (project part 17) and the European Union in the frame of the Cold Molecules TMR Network under Contract No. HPRN-CT-2002-00290.

APPENDIX: THEORETICAL MODEL AND FIT PARAMETERS

We use a theoretical model by Bohn and Julienne [16] to fit the data in Figs. 4–7. In the following we give a short summary of this model and present the procedure to calculate the scattering matrix S, the loss coefficient K_{inel}, and the scattering length a. The model has the advantage that it is concise and intuitive and it allows treatment of multilevel systems with several couplings between the levels. The numerical calculations involve simple manipulations of small matrices.

In Fig. 8 the level scheme for our two models involving four and six levels are shown. We first restrict our description to the four-level model as shown in the right part of Fig. 8. In this way our description stays compact and matrices are kept small. The extension to six or more levels follows the same scheme.

Four-level model

Compared to Fig. 1 an additional excited level $|3\rangle$ is added. This level corresponds to the rotational level $J=0$ and lies 290 MHz below the $J=2$ rotational level $|1\rangle$ [9]. We work in the dressed atom picture and every level $|i\rangle$ is attributed a detuning Δ_i (see Fig. 8). Δ_0 is arbitrarily set to 0. The transition strengths from the continuum $|0\rangle$ to levels $|1\rangle$ and $|3\rangle$ are described by stimulated rates Γ_{01} and Γ_{03} which are proportional to the intensity I_1 of laser 1. The transitions between the bound levels $|2\rangle$ and $|1\rangle,|3\rangle$ are characterized by the Rabi frequencies Ω_{12} and Ω_{23}, respectively, which are

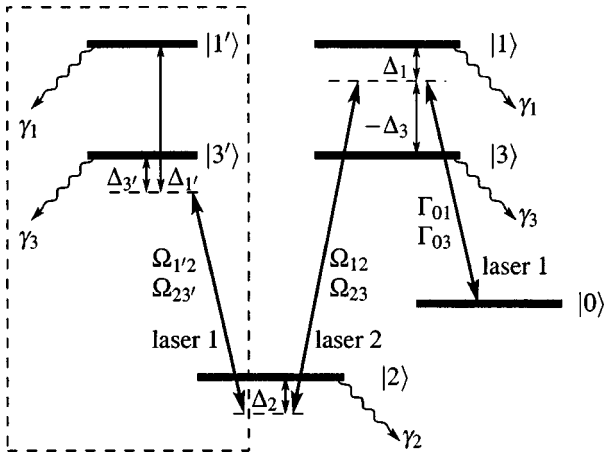

FIG. 8. Extended level scheme (compare to Fig. 1) for the four-level model (right-hand side) and its extension with six levels. State $|3\rangle$ corresponds to the $J=0$ level and lies 290 MHz below the $J=2$ level $|1\rangle$. The four-level model is based on levels $|0\rangle,|1\rangle,|2\rangle$, and $|3\rangle$. The auxiliary levels $|1'\rangle$ and $|3'\rangle$ are introduced in the extended model to describe the coupling between $|2\rangle$ and $|1\rangle,|3\rangle$, respectively, due to laser 1 (see text).

proportional to $\sqrt{I_2}$. Spontaneous decay from the bound levels leading to atomic losses is formally taken into account by introducing artificial levels $|a_i\rangle$ for each level $|i\rangle$ to which a transition at rate γ_i takes place (not shown in Fig. 8). All these couplings between different levels are summarized in the symmetric reaction matrix K. We arrange the level names in the order $(0, a_1, a_2, a_3, 1, 2, 3)$ and use them as row and column indices. The nonzero matrix elements of the K matrix then read $K_{01}=\sqrt{\Gamma_{01}/2}$, $K_{03}=\sqrt{\Gamma_{03}/2}$, $K_{ia_i}=\sqrt{\gamma_i/2}$, $K_{12}=\Omega_{12}$, and $K_{23}=\Omega_{23}$. Levels 0, a_1, a_2, and a_3 are referred to as open channels, levels 1, 2, and 3 as closed channels. The reaction matrix K is partitioned into open and closed channel blocks,

$$K=\begin{pmatrix} \mathbf{0} & K^{\mathrm{oc}} \\ K^{\mathrm{co}} & K^{\mathrm{cc}} \end{pmatrix}.$$

K^{oc} reads in our case

$$K^{\mathrm{oc}}=\begin{pmatrix} \sqrt{\Gamma_{01}/2} & 0 & \sqrt{\Gamma_{03}/2} \\ \sqrt{\gamma_1/2} & 0 & 0 \\ 0 & \sqrt{\gamma_2/2} & 0 \\ 0 & 0 & \sqrt{\gamma_3/2} \end{pmatrix}.$$

K^{co} is the transposed matrix of K^{oc} and

$$K^{\mathrm{cc}}=\begin{pmatrix} 0 & \Omega_{12} & 0 \\ \Omega_{12} & 0 & \Omega_{23} \\ 0 & \Omega_{23} & 0 \end{pmatrix}.$$

From K the reduced K matrix

$$K^{\mathrm{red}}=K^{\mathrm{oc}}(D-K^{\mathrm{cc}})^{-1}K^{\mathrm{co}}$$

is calculated, eliminating the closed channels 1–3, where D denotes a diagonal matrix with diagonal elements

$(\Delta_1, \Delta_2, \Delta_3)$. This determines the unitary 4×4 scattering matrix S:

$$S = (\mathbf{1} + iK^{\mathrm{red}})(\mathbf{1} - iK^{\mathrm{red}})^{-1}.$$

From the matrix elements S_{ij} of S the trap loss coefficient K_{inel} is calculated by

$$K_{\mathrm{inel}} = \frac{\pi\hbar}{\mu k_{\mathrm{i}}} \sum_i |S_{0a_i}|^2 = \frac{\pi\hbar}{\mu k_{\mathrm{i}}}(1 - |S_{00}|^2),$$

where $\mu = m_{\mathrm{Rb}}/2$ is the reduced Rb mass and $\hbar k_{\mathrm{i}}$ the relative momentum of the colliding atoms. The scattering length is obtained from S_{00} via

$$a = a_{\mathrm{bg}} - \frac{1}{2k_{\mathrm{i}}} \frac{\mathrm{Im}(S_{00})}{\mathrm{Re}(S_{00})},$$

where $\mathrm{Re}(S_{00})$ and $\mathrm{Im}(S_{00})$ denote the real and imaginary parts of S_{00}, respectively.

In the limit of small relative momentum $\hbar k_{\mathrm{i}}$ and small coupling strengths $\Gamma_{0i} \ll \gamma_i$, K_{inel} and the light-induced change of the scattering length $a - a_{\mathrm{bg}}$ are independent of k_i because the Γ_{0i} are proportional to k_{i} (Wigner threshold regime) [16].

Extension of the four-level model

The four-level model neglects that laser 1 (of which the intensity is typically 5 times greater than that of laser 2) also couples the levels $|2\rangle$-$|1\rangle$ and $|2\rangle$-$|3\rangle$. However, this coupling should be taken into account since laser 1 is not far detuned from these transitions (see Fig. 8) due to the small binding energy of state $|3\rangle$ ($636\ \mathrm{MHz}\times h$) which is comparable to typical detunings Δ_1. It mainly leads to broadening and light shifting of level $|2\rangle$. The additional coupling can approximately be taken care of by adding another two auxiliary levels $|1'\rangle$ and $|3'\rangle$ with detunings $\Delta_{1'} = \Delta_1 + \Delta_2 + 2\pi \times 636$ MHz and $\Delta_{3'} = \Delta_3 + \Delta_2 + 2\pi \times 636$ MHz as shown in Fig. 8. The coupling strengths $\Omega_{1'2}$ and $\Omega_{23'}$ are fixed by $\Omega_{1'2} = \Omega_{12}\sqrt{I_1/I_2}$ and $\Omega_{23'} = \Omega_{23}\sqrt{I_1/I_2}$. Compared to the four-level model no new fit parameters are introduced. We can calculate K_{inel} and the scattering length a following the same recipe as for the four-level model, only with larger matrices. Fitting the data in Figs. 4–7 this extended model produced much better results than the four-level model. For completeness we give here the fit parameters which were used in the calculations in Figs. 5–7 ($I_1 = 300\ \mathrm{W/cm^2}$ and $I_2 = 60\ \mathrm{W/cm^2}$): $\Gamma_{01}/2\pi = 42$ kHz, $\Gamma_{03}/2\pi = 8$ kHz, $\Omega_{12}/2\pi = 32$ MHz, $\Omega_{23}/2\pi = 12$ MHz, $\gamma_1/2\pi = 25$ MHz, $\gamma_3/2\pi = 22$ MHz, and $\gamma_2/2\pi = 2$ MHz. We used $k_{\mathrm{i}} = 2.5\times10^{-5}\ \mathrm{m^{-1}}$. Due to the limitations of our model, these fit parameters should not be mistaken as the true values of the corresponding physical quantities.

[1] E. Tiesinga, B. J. Verhaar, and H. T. C. Stoof, Phys. Rev. A **47**, 4114 (1993).

[2] S. Inouye *et al.*, Nature (London) **392**, 151 (1998); Ph. Courteille, R. S. Freeland, D. J. Heinzen, F. A. van Abeelen, and B. J. Verhaar, Phys. Rev. Lett. **81**, 69 (1998); J. L. Roberts *et al.*, *ibid.* **81**, 5109 (1998).

[3] C. Chin, V. Vuletic, A. J. Kerman, and S. Chu, Phys. Rev. Lett. **85**, 2717 (2000); A. Marte *et al.*, *ibid.* **89**, 283202 (2002).

[4] E. A. Donley, N. R. Claussen, S. T. Thompson, and C. E. Wieman, Nature (London) **417**, 529 (2002).

[5] L. Khaykovich *et al.*, Science **296**, 1290 (2002); K. E. Strecker, G. B. Partridge, A. G. Truscott, and R. G. Hulet, Nature (London) **417**, 150 (2002).

[6] S. L. Cornish, N. R. Claussen, J. L. Roberts, E. A. Cornell, and C. E. Wieman, Phys. Rev. Lett. **85**, 1795 (2000); T. Weber, J. Herbig, M. Mark, H.-C. Nägerl, and R. Grimm, Science **299**, 232 (2003).

[7] S. Jochim *et al.*, Science **302**, 2101 (2003); M. Greiner, C. A. Regal, and D. S. Jin, Nature (London) **426**, 537 (2003); M. Zwierlein *et al.*, Phys. Rev. Lett. **91**, 250401 (2003); T. Bourdel *et al.*, *ibid.* **93**, 050401 (2004).

[8] C. A. Regal, M. Greiner, and D. S. Jin, Phys. Rev. Lett. **92**, 040403 (2004); M. W. Zwierlein *et al.*, *ibid.* **92**, 120403 (2004); C. Chin *et al.*, Science **305**, 1128 (2004).

[9] M. Theis *et al.*, Phys. Rev. Lett. **93**, 123001 (2004).

[10] F. K. Fatemi, K. M. Jones, and P. D. Lett, Phys. Rev. Lett. **85**, 4462 (2000).

[11] P. O. Fedichev, Y. Kagan, G. V. Shlyapnikov, and J. T. M. Walraven, Phys. Rev. Lett. **77**, 2913 (1996).

[12] J. L. Bohn and P. S. Julienne, Phys. Rev. A **56**, 1486 (1997).

[13] R. Wynar, R. S. Freeland, D. J. Han, C. Ryu, and D. J. Heinzen, Science **287**, 1016 (2000).

[14] T. Rom *et al.*, Phys. Rev. Lett. **93**, 073002 (2004); Ch. Lisdat, N. Vanhaecke, D. Comparet, and P. Pillet, Eur. Phys. J. D **21**, 299 (2002).

[15] J. Stenger *et al.*, Phys. Rev. Lett. **82**, 4569 (1999).

[16] J. L. Bohn and P. S. Julienne, Phys. Rev. A **60**, 414 (1999).

[17] M. Greiner, I. Bloch, T. W. Hänsch, and T. Esslinger, Phys. Rev. A **63**, 031401 (2001).

[18] T. Esslinger, I. Bloch, and T. W. Hänsch, Phys. Rev. A **58**, R2664 (1998).

[19] A. Fioretti *et al.*, Eur. Phys. J. D **15**, 189 (2001).

[20] E. Tiemann (private communication).

[21] P. Julienne and E. Tiesinga (private communication).

[22] P. S. Julienne, F. H. Mies, E. Tiesinga, and C. J. Williams, Phys. Rev. Lett. **78**, 1880 (1997).